Numerical assessment of concrete damage: Procedures and pitfalls

P. Stroeven and He Huan
Delft University of Technology, the Netherlands

The paper focuses on the quality of predicting the damage characteristics of the loaded engineering structure by subjecting section images of cores supposedly drawn from the concrete of the structure to quantitative image analysis by sweeping test lines. Automation of this data acquisition stage is shown, generally leading to information that is biased to an unknown degree. This is accomplished mathematically and graphically according to Underwood. When the Stroeven/Saltikov (S/S)-concept of a partially linear-planar model for damage is accepted and (four-connexity) digitization is accomplished in a direction adjusted to the prevailing orientation direction of the cracks, the paper shows that orthogonal observations in vertical sections are sufficient for the unbiased assessment of total crack length per unit of area (2D), or specific crack surface area (3D), also when digitized images are employed. This is possible in situations where (uniaxial) compressive or tensile stresses dominate. The crack orientation distribution is however always biased when determined on digitized images in an automated set up when pixel directions are not compensated for, such as by the quantified S/S-concept of damage.

Key words: Computers, concrete, damage, digitization, multi-stage sampling, quantitative image analysis

1 Introduction

Studying the material structure of concrete requires time-consuming and expensive experimental efforts. Therefore, concrete is increasingly made in virtual reality, yielding the so-called compucrete. Modern computer technology renders possible realistically simulating the real material, the realcrete. Discrete element modeling (DEM) based on concurrent algorithms is used for this purpose [Bentz *et al.* 1993; Fu and Dekelbab 2003; Grutzeck *et al.* 1993; Tsunekawa and Iwashita 2001; Stroeven and Guo 2006; He 2010]. Concrete is not perfect. Even in the virgin state it can contain myriads of tiny cracks that form the starting point of damage evolution under load. Also durability risks are

associated with the formation of a spatial network of such cracks. The quantitative assessment of the geometrical statistical features of such network structures has been targeted in experimental as well as in DEM research [Chen *et al*. 2006; Stroeven and Guo 2006]. Both approaches rely on a similar methodology to achieve this goal, *i.e.*, *quantitative image analysis* (QIA). Simple observations are performed in section planes such as counting intersections with a sweeping line grid. Both approaches yield similar information that is transformed into 3D damage characteristics when experiments are based on a proper sampling scheme. This methodology is well-known nowadays.

The paper will focus on the partially linear-planar damage model to achieve such goals in an economic and reliable way. This way of approach has been introduced earlier [Stroeven 1979;1982;1990;2009]. Introduction of the computer to take over the simple but somewhat time-consuming handwork in QIA operations applied to experimental or DEM cases could be a bad choice, since automation may lead to seriously *biased* information as will be demonstrated mathematically and graphically, following Underwood [1970]. Such biases have also been discussed in a slightly different way by Chaix and Grillon [1996]. The QIA methodology is available, however for implementation extensive time and labor investments are required. Hence, introduction of the computer is tempting and therefore the common approach nowadays. So, researchers should be aware of the risks of introducing serious biases in the observations. This paper points the researcher's attention to such biases. Moreover, a way out of this dilemma is discussed. The consequences of introducing the computer for automation of the QIA stage constitute therefore the hard core of the paper.

The ultimate engineering goal of such research efforts would be developing the ability to more reliably predict the behavior of full-scale reinforced concrete structures. The QIA data would be the last stage in a multi-stage sampling process. Successively, one may emphasize cores drawn from the full-size structure (locations, orientations and numbers are crucial elements in the first sampling stage). The cores have to be sectioned in the second sampling stage (with similar crucial decisions to be taken). Field images with representative status have to be prepared in the third sampling stage from the section images. The next and fourth sampling stage involves the data acquisition process. Overall scatter should be minimized in this four-stage sampling design. Studies on these aspects have demonstrated that an increase in the number of cores would be more efficient than enhancing the number of intersections of cracks and grid lines. This is popularly expressed by the saying: "*Do more less well*" [Gundersen and Osterby 1981]. This speaks also against

the risky involvement of the computer in stage four, because of the relatively low demand on time and labor investments in the QIA operation.

2 Damage assessment by QIA

Damage evolves due to external and internal loads to which the concrete structure is subjected. Even before major cracks are formed that can seriously violate the reliability of the engineering structure, one may be interested in assessment of the state of damage that has been developed so far. It should be mentioned that damage is a *fractal* phenomenon [Wang and Diamond 2001], so one should assess the magnification by which section (or field) images are prepared. Improving magnification leads to a denser pattern of observable cracks [Ringot and Bascoul 2001; Saouma *et al.* 1990; Stroeven 2009] and rougher fracture surfaces [Carpinteri and Puzzi 2009]. The methodology of damage assessment on sections of cores drawn from the structure (or of specimens used in laboratory research) is already available for quite some time. It involves a proper sampling design by sections, careful preparation of the section images after sawing (polishing, contrast improvement, assessment of magnification) and possibly image modifications, such as by digitization, skeletonization, etc. [Darwin *et al.* 1995; Ammouche *et al.* 2000]. In general, *random sampling* would be required to get unbiased 3D damage information [Howard and Reed 2005]. This is very unpractical and would offer a highly uneconomical approach. Hence, researchers limit themselves generally to two-dimensional (2D) investigations only [Wulfsohn *et al.* 2004; Maletti and Wulfsohn 2006]. Due to the 3D nature of the concrete structure this is not a very realistic approach, which can easily lead to misleading conclusions. So, this paper presents an alternative by the so called S/S-concept; this is not new either, but unfortunately largely neglected. Major focus will be on quantification of the biases introduced by digitization that is at the basis of (semi-) automation of the image analysis stage. Further, a way out of such problems will be indicated.

Damage in concrete constitutes a spatial network structure of partly connected crack surfaces (representing two crack surfaces at very small distances), so that section images reveal a pattern of partly connected cracks as lineal features. This spatially complex damage structure that should be analysed in stage 4 can be conceived according to the S/S-concept [Stroeven 1982] as a *partially linear-planar structure*. The 3D portion encompasses (infinitely) small *flat* crack elements dispersed isotropic uniformly random (IUR) in space. In the 2D portion, similar small flat crack elements are collected that are parallel to an

orientation plane, however otherwise they are "randomly" distributed. The 1D portion encompasses small flat crack elements that are all parallel to an orientation axis and otherwise "randomly" dispersed. So, a real crack is hypothetically sub-divided into such small flat elements, which will find a place in one or more of these portions. When the 2D portion can be neglected, a so called *partially linearly oriented* system is obtained. This model can be used in situations where compressive stresses are prevailing. Alternatively, for high tensile stresses the *partially planar oriented* damage model can be employed in which the 1D portion is neglected.

Crack density is commonly expressed in total surface area, S, per unit of volume, V. So, leading descriptor of the damage structure is S_V (=S/V in mm^{-1}). Alternatively, in 2D the total crack length L per unit of area A yields information on L_A (=L/A in mm^{-1}). Measurements are made upon superposition of line grids on images, of which Fig. 1 (left) reveals only a small part (pore is visible at the bottom). Contrast was improved in this case by applying a fluorescent spray. The first author has extensively used this method of directed secants in the past 30 years [Nemati and Stroeven 2000; Reinhardt *et al*. 1978; Stroeven 1979, 1990; Stroeven and Hu 2007]. Incidentally, it was also employed by other researchers in concrete technology [Carcassès *et al*. 1989; Nemati 1994; Ringot 1988; Stang *et al*. 1990]. Fig. 1 (right) shows grid orientations on a full-size hand-made copy of cracks detectable by naked eye on a section image of a prismatic specimen subjected to compression (in longitudinal direction). Larger aggregate grains are visible as crack-free areas. This picture may demonstrate the complexity of the crack structure and the high density of cracks under relatively high compression loading (a major part of cracks was already developed in the virgin state of the material), whereby no major crack formation (process zones) could be observed [Stroeven 1979].

The cracks in the section image can have a prevailing orientation that is unknown and thus deviating from a Cartesian coordinate direction. This more general case has been elaborated extensively elsewhere [Stroeven *et al*. 2001;2005]. In the present case it is assumed that the crack pattern in the section images can be properly oriented with respect to the Cartesian coordinate system, so that digitization required for an automated set up can be adjusted to this coordinate system. This situation occurs in material research in the laboratory where specimens are subjected to simple loading regimes, like uniaxial compression or uniaxial tension. For section images of cores this would be less easy, but at least approximately this can be arranged for situations in which either compressive or tensile stresses prevail. Otherwise the aforementioned approach should be followed.

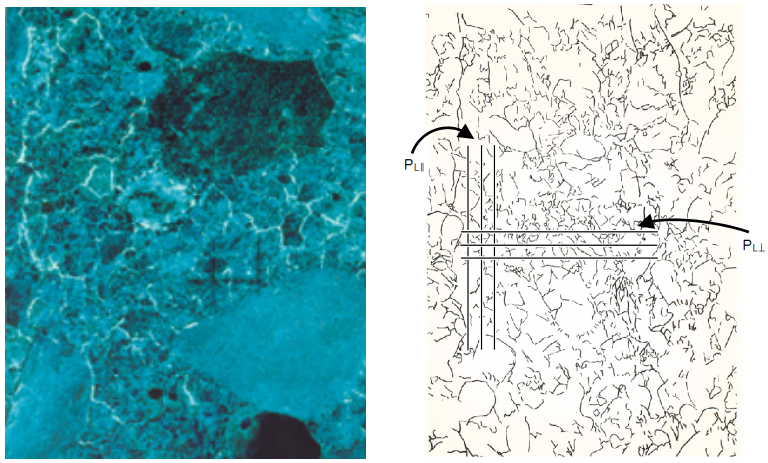

Figure 1: Compression loading-induced cracks visualized by fluorescent spray. At the right, the analogue image of the visible crack pattern in the central part of a vertical section of a prismatic specimen (width about 100mm) subjected to the directed secants method. Cracking at a small part of this vertical section is revealed by the micrograph image at the left that is taken at only modest magnification (light-colored sand grain and dark-colored pore are displayed at the bottom right).

2.1 ***Prevailing compressive stress field in concrete***

Uniaxial compressive stresses produce predominantly cracks that are parallel to the loading direction. This is particularly apparent at low observation sensitivity (at low magnification). In a more general set up, we assume a portion of cracks distributed isotropic uniformly random (IUR); this is denoted as the S_{V3} component. The remaining portion consists of cracks parallel to the orientation (=loading) axis, denoted as the S_{V1} component. Total crack density in this *partially linearly oriented* system is the summation of both components: $S_{V1} + S_{V3} = S_V$. The proper approach (in technical as well as economic terms) is sampling by *vertical sections*. Hence, the specimen should be cut to yield one or more image planes parallel to the orientation axis. Such section images can provide the 3D information on S_V. Averaging over more vertical images reduces the scatter around the average, and thus the reliability of the results. The results are unbiased, which means that averaging over an increasing number of images will bring the average closer and closer to the population value we are interested in. The analysis of the images is accomplished by line scanning. A grid of parallel lines is superimposed on the crack pattern, successively in the direction of the orientation axis (indicated by index $\|$) and perpendicular to it

(indicated by index $\perp$), as shown in Figs. 1 and 2. The following relationships are readily available in the international literature, such as in Stroeven [1990]:

$$P_{L\parallel} = \tfrac{1}{2} S_{V3} \quad \text{and} \quad P_{L\perp} = \tfrac{1}{2} S_{V3} + \tfrac{2}{\pi} S_{V1} \tag{1}$$

Hence, crack density (specific crack surface area) is obtained by simple mathematical manipulations, yielding:

$$S_V = \tfrac{1}{2}\pi P_{L\perp} + (2 - \tfrac{1}{2}\pi) P_{L\parallel} \tag{2}$$

P in Eqs. (1) and (2) stands for the number of intersections of grid lines (with total length L) and cracks. The constants (*i.e.*, $1/2$ and $2/\pi$) account for the combined probabilities of 3D cracks intersecting the section plane and thereupon the line grid. Interested readers can find the analytical derivations in Stroeven and Hu [2007] and in Nemati and Stroeven

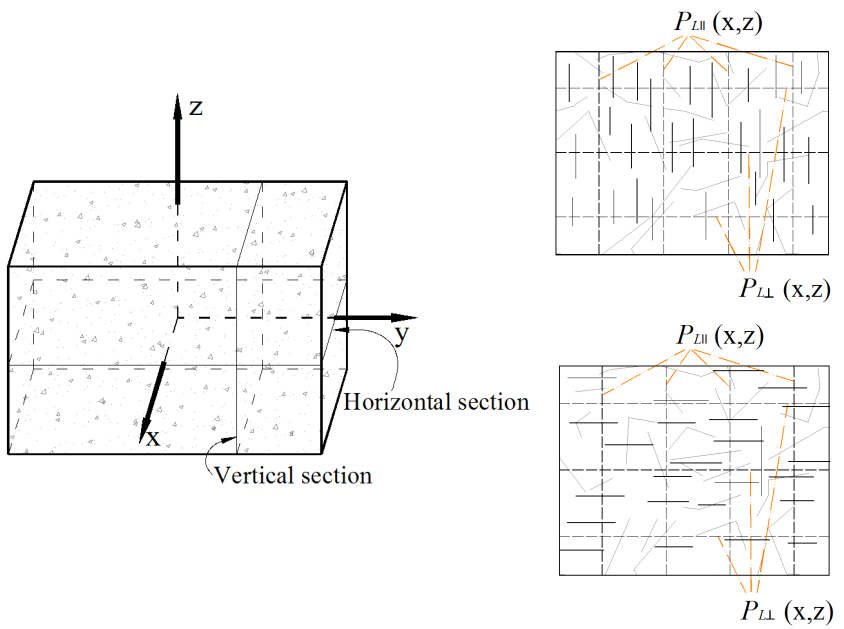

Figure 2: Intersection counting of cracks in vertical sections of concrete revealing partially linear (top: compression case) and partially planar crack orientation (bottom: tension case) with grids oriented in orthogonal directions (dashed lines). Cracks are displayed in vertical section images by dark lines (=2D linear portion) and grey lines (2D "random" portion).

[2001]. Yet, the procedure of deriving the expressions in Eq. (1) will be shortly discussed to get familiar with the geometrical statistical nature of reasoning. The unit sphere model displayed in Fig. 3 is employed for this purpose.

A total number of N parallel test lines are randomly spaced in a cube with linear dimension l. Small flat crack elements of the 2D portion are also randomly dispersed parallel to the orientation plane and perpendicular to the test lines. Number of intersections of lines and cracks is denoted by P. Ratio of P and N equals area fraction of the cracks according to the point counting method [Underwood 1970; Stroeven 1973]. Hence, $P/N = A/A_{tot} = S_2 l / V_{tot}$. Herein, S_2 represents the total surface area of crack elements in the 2D portion. $P / l.N = P_{L\perp} = S_2 / V_{tot} = S_{V2}$ is readily obtained after reorganization of parameters. The total projection on the bottom of the cube (which is perpendicular to the test lines) of the small flat crack elements ΔS of the 3D portion should be determined for derivation of the expression at the left of Eq. (1). The unit sphere in Fig. 3 displays at its surface in their original spatial orientation all small flat crack elements ΔS. The vertical projection of these crack elements is governed by $\cos\theta \cdot \Delta S$. The number of crack elements similarly oriented (enclosing the same angle θ with the vertical axis) is according to the unit sphere model proportional to $\sin\theta$ as depicted by Fig. 3. The total projection of all small flat crack elements of the 3D portion therefore amount to half its original size, so $S=2A$. This results from the expression: $\int \sin\theta \cos\theta d\theta / \int \sin\theta d\theta$. As a

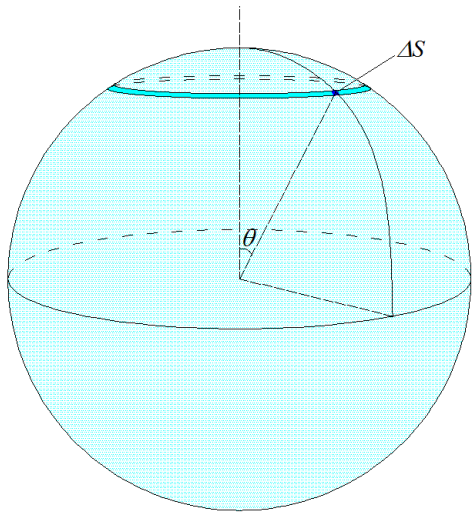

Figure 3: Unit sphere model showing infinitely small crack element from IUR damage system

consequence, $P_L = S_{V3}/2$. For the 1D portion, the relevant total projection operation leads to an area reduction of: $\int \cos\theta d\theta / \int d\theta = 2/\pi$. Hence, $P/l.N = P_{L\perp} = 2/\pi \cdot S/V = 2/\pi S_{V1}$.

2.2 *Prevailing tensile stress field*

The methodology is very similar. The vertical section is parallel to the loading direction. The grid is also successively superimposed in the loading direction and perpendicular to it, with the same indices accounting for the position of the grid. In this case we have:

$$P_{L\|} = \frac{1}{2} S_{V3} + S_{V2} \quad \text{and} \quad P_{L\perp} = \frac{1}{2} S_{V3} \tag{3}$$

Again, simple manipulation will yield:

$$S_V = S_{V2} + S_{V3} = P_{L\|} + P_{L\perp} \tag{4}$$

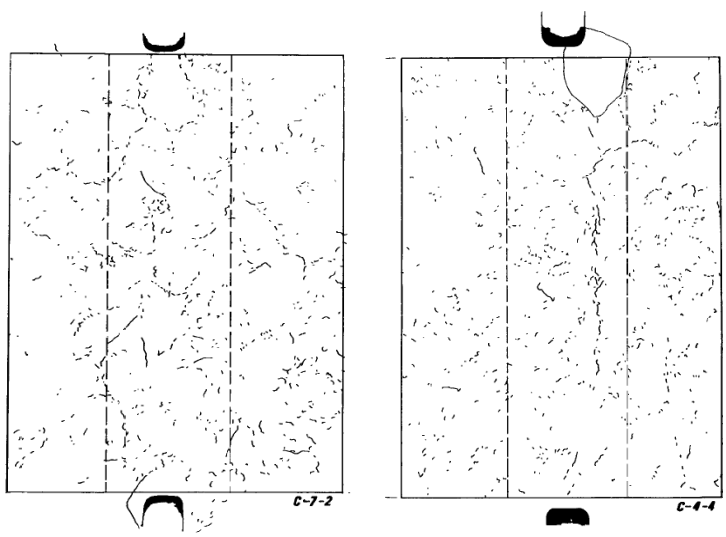

(a) (b)

Figure 4: Damage states in vertical sections of central part of two-sided notched prismatic concrete specimen (with 50 mm between the notches visible at top and bottom) subjected to uniaxial tensile stresses (horizontal direction) along descending branch (a): about three quarter of ultimate, and (b): about halfway down. Contrast was improved by a fluorescent spray. For additional experimental details, see Stroeven [1990].

Here, S_{V2} stands for the portion of cracks perpendicular to the loading axis, with $S_V = S_{V2} + S_{V3}$. To accomplish such operations, the contrast should be improved by ink penetration or by application of a fluorescent spray (as in the case of Fig. 1) or dye. Details on analytical manipulations can be found in the relevant literature [Reinhardt *et al*. 1978; Stroeven 1990; Stroeven and Hu 2007]. Fig. 2 also offers a sketch of the geometrical statistical situation underlying the intersection case of the 2D portion. Fig. 4 may demonstrate that even under moderate magnifications (say 5-10 times), major crack concentration in a fracture process zone occurs well over the top of the stress-strain curve of a two-sided notched prismatic specimen.

3 Analogue versus digitized images

3.1 Analogue images

An elegant way to reveal differences in outcomes of quantitative image analysis approaches by directs secants (line scanning) to analogue and (four-connexity) digitized images is to make use of the earlier mentioned S/S-concept. Hence, L_A is assumed consisting of two portions, a "random" one, denoted by L_{Ar}, and a fully oriented one, indicated by L_{Ao}. The latter "sticks" (short straight elements as part of the 2D cracks) run parallel to the orientation axis that supposedly coincides with the positive x-axis. This strategy allows dealing with both portions separately. The rose of intersections per unit of grid line length (intersection densities) of the random portion approximates (for very large images) a circle around the origin with radius P_{Lr} (Fig. 5 at the right). The rose of intersection densities for the oriented portion is a circle through the origin (Fig. 5 at the left). Its main extension is $P_{Lo}(\theta = \pi/2) = P_{Lo\max}$, so perpendicular to the orientation direction of the sticks in the oriented portion. When combined, the rose of intersection densities is obtained for a partially linear structure of lineal features in a plane, shown in Fig. 6 [Stroeven 1979]. The intersection density in an arbitrary direction is:

$$P_L(\theta) = P_{Lr} + P_{Lo\max} \sin\theta \tag{5}$$

It is readily seen that for $\theta = \pi/2$ the total rose takes its maximum value, so cracks are oriented parallel to the x-axis. Note that the 2D portion in the image plane can originate from the linear portion in compression or from the planar portion in tension. Hence, both situations are described.

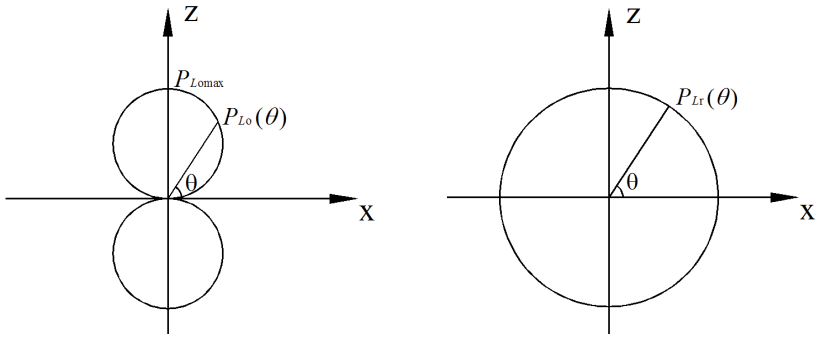

Figure 5: Rose of intersection densities for oriented (left) and random (right) line segments in a plane (together forming the 2D crack pattern) for an analogue image

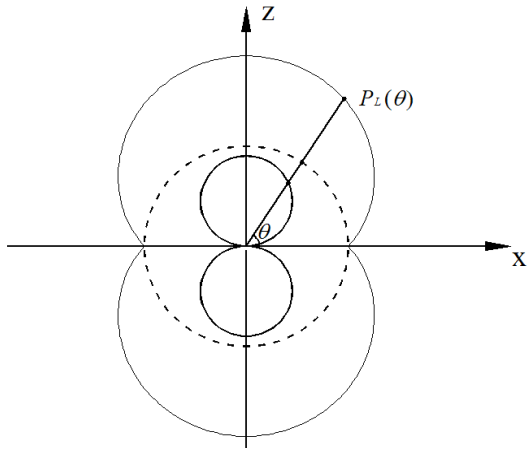

Figure 6: Rose of intersection densities for random (dashed line) plus oriented line segments in a plane (continuous line; small circles) shown in Fig. 5

3.2 ***Digitized images***

The smooth contours of the cracks can be conceived in conventionally digitized images replaced by two orthogonal sets of mono-size sticks as shown in Fig. 7. As before, a distinction is made between the "random" portion and the oriented one. The random portion in the digitized image consists of two equally large sub-sets of sticks oriented in the respective coordinate directions {*x, z*}. This leads to two equally large roses of intersection densities that run through the origin and are orthogonally oriented. Circle diameter is P_{Lr}. The summation yields a symmetric flower-like rose displayed in Fig. 8 at the left.

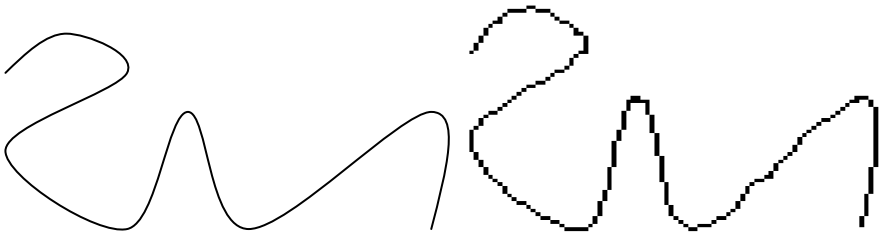

Figure 7: Smoothly curved crack in analogue image (left) is replaced in conventionally digitized image by an orthogonal set of straight line segments (right).

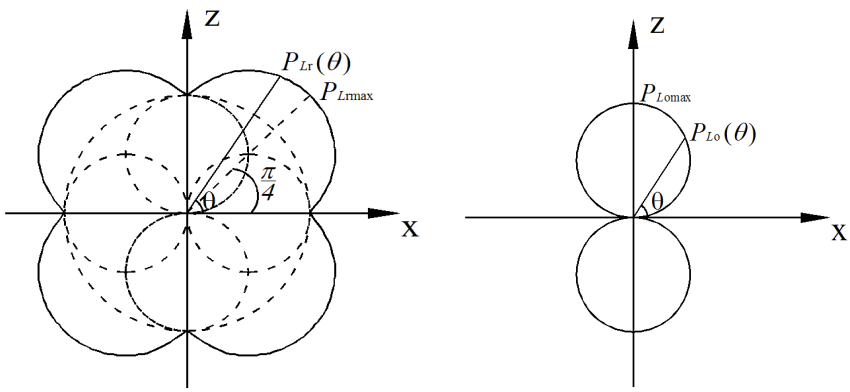

Figure 8: Rose of $P_L(\theta)$ values for random (left) and oriented (right) line segments in digitized image of crack pattern.

In an arbitrary direction, the intersection density is given by:

$$P_{Lr}(\theta) = P_{Lr}(\sin\theta + \cos\theta) = \sqrt{2}P_{Lr}\left|\cos(\theta - \tfrac{1}{4}\pi)\right| \tag{6}$$

A striking but expected observation is that the preferred orientation direction encloses an angle $\pi/4$ with the positive x-axis; the random portion is reflected significantly biased by a flower-like curve around the origin with maximum value $\sqrt{2}P_{Lr}$.

The oriented portion in the digitized image gives rise to a similar rose of intersection densities as in the analogue case. Hence, the intersection density in an arbitrary direction θ is given by:

$$P_L(\theta) = P_{Lo\max}\sin\theta + \sqrt{2}P_{Lr}\left|\cos(\theta - \tfrac{1}{4}\pi)\right| \tag{7}$$

The direction of the principal axis of the total rose is found for zero value of the first derivative of Eq. (7). This leads to $\mathrm{tg}\,\theta = (P_{Lr} + P_{Lo\,\max})/P_{Lr}$. Hence, for only random cracks the principal direction of orientation is under 45^0 with the positive x-axis. For only the oriented portion, we have $\theta = \pi/2$; cracks run in the x-direction. However, for the practical case of partial orientation data, the principal direction of orientation will be anywhere between these two values. Hence, results are biased to an unknown degree.

4 Biases due to automation in crack extension

Total crack length is readily obtained by application of $L_A = \frac{1}{2}\pi \bar{P}_L(\theta)$. This yields for:

$$\textit{Analogue image: } L_A = \frac{\pi}{2}\frac{\int_0^{\pi/2}(P_{Lr} + P_{Lo\max}\sin\theta)d\theta}{\int_0^{\pi/2}d\theta} = \frac{\pi}{2}P_{Lr} + P_{Lo\max} \tag{8}$$

$$\textit{Digitized image: } L_A = \frac{\pi}{2}\frac{\int_0^{\pi/2}(P_{Lr}\sin\theta + P_{Lr}\cos\theta + P_{Lo\max}\sin\theta)d\theta}{\int_0^{\pi/2}d\theta} = 2P_{Lr} + P_{Lo\max} \tag{9}$$

L_A as obtained from digitized image is *always biased* (*i.e.*, overestimated). Only for extremely oriented cracks the obtained data approximate the correct value. For only random cracks the data overestimate the total crack length by a factor $4/\pi$. For mixed situations, the bias can be anywhere between 1 (unity) and $4/\pi$. For spatial information, use could be made of the relationship $S_V = 2\bar{P}_L$, but data derived from application of sweeping test lines on digitized vertical section images can neither be used for reliably predicting specific crack surface area.

However, we should stress that when the direction of preferred orientation of the damage structure can be estimated sufficiently accurate, as assumed so far, the adoption of the S/S-concept would also offer a reliable solution for digitized images! This is because structural characteristics like total crack length and specific crack surface area can be exclusively related to orthogonal observations in vertical sections. Fig. 9 may demonstrate that the random crack portion is measured correctly in orthogonal directions (adjusted to the direction of four-connexity digitization!), so L_A and S_V can be assessed in an unbiased way.

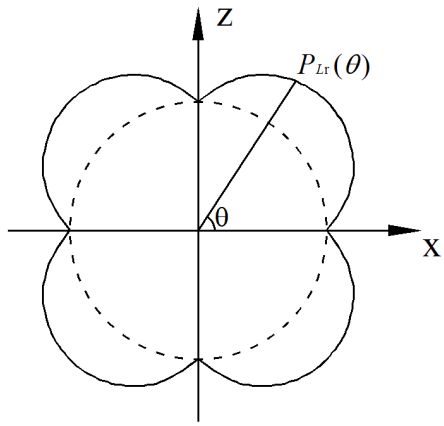

Figure 9: Digitization-induced biases for random portion of rose of intersection densities. Dashed line represents the analogue image, the solid line the digitized image.

Eqs. (2) and (4) transform the orthogonal observations made in the 2D image plane of a vertical section to the 3D reality. In the analogue and digitized image, we find for the tension and compression cases:

$$\begin{aligned} &\textit{(tension)} \quad P_{L\|} = P_{Lr} \quad \textit{and} \quad P_{L\perp} = P_{Lr} + P_{Lo\max} \\ &\textit{(compression)} \quad P_{L\perp} = P_{Lr} \quad \textit{and} \quad P_{L\|} = P_{Lr} + P_{Lo\max} \end{aligned} \tag{10}$$

For the tension case this leads according to Eq. (4) to:

$$S_V = P_{L\perp} + P_{L\|} = 2P_{Lr} + P_{Lo\max} \tag{11}$$

Similarly, according to Eq. (2), we find for the compression case:

$$S_V = \tfrac{1}{2}\pi P_{L\perp} + (2 - \tfrac{1}{2}\pi) P_{L\|} = 2P_{Lr} + \tfrac{1}{2}\pi P_{Lo\max} \tag{12}$$

When the portions of cracks have been assessed from vertical sections, either on analogue or digitized images, the spatial orientation distribution is governed by the S/S-concept. The 2D orientation distribution of crack length is as an example given in Eq. (8) for the tension case, as illustrated at the right hand side of Fig. 6, and yields:

$$L_A(\theta) = P_{Lr} + P_{Lo\max} \sin\theta \tag{13}$$

Similarly, in 3D space for the tension case:

$$S_V(\theta,\beta) = (P_{Lr} + P_{Lo\max} \sin\theta)\cos\theta \tag{14}$$

Executing the averaging operation for the tension case, we find:

$$S_V(\theta,\beta) = 2\overline{P}_L = 2\frac{\int_0^{\pi/2}\int_0^{\pi/2}(P_{Lr} + P_{Lo\max})\cos\theta\, d\theta\, d\beta}{\int_0^{\pi/2}\int_0^{\pi/2}\cos\theta\, d\theta\, d\beta} \tag{15}$$

yielding the same expression as in Eq. (11). Similarly, for the compression case:

$$S_V(\theta,\beta) = 2\overline{P}_L = 2\frac{\int_0^{\pi/2}\int_0^{\pi/2}(P_{Lr} + P_{Lo\max}\cos\theta)\cos\theta\, d\theta\, d\beta}{\int_0^{\pi/2}\int_0^{\pi/2}\cos\theta\, d\theta\, d\beta} \tag{16}$$

providing also the correct expression given in Eq. (12).
Note that the cracks in the vertical plane due to the 1D (compression) and 2D (tension) portions are orthogonal, so also the Underwood circles are orthogonally oriented. This leads to the cosine and sine functions in Eqs. (15) and (16), respectively (*i.e.*, $L_A(\theta) = P_{Lr} + P_{Lo\max}\cos\theta$ for the compression case).

5 Multi-stage sampling scheme

To predict behavior of concrete in the engineering structure, we have to sample on different levels. Successively, one may emphasize cores drawn from the full-size structure (locations, orientations and numbers are crucial elements in the first sampling stage). The cores have to be sectioned in the second sampling stage (with similar crucial decisions to be taken). Field images with representative status have to be prepared in the third sampling stage. The next and fourth sampling stage concerns the data acquisition on the field images. Overall scatter should be minimized in this four-stage sampling design. This

illustrates convincingly that reduction of scatter in one sampling stage significantly below the level in one or more other stages will have no sense, moreover leading only to negative economic impact.

Since the number of cores representing similar conditions in the concrete structure will be very limited, the between-cores scatter will dominate the multi-stage sampling scheme. Moreover, preparation of a large number of (vertical) sections from core samples will be a laborious and thus expensive undertaking. Additionally, the contrast between cracks and background has to be improved per vertical section by ink, fluorescent or dye penetration: another argument for limitation of the number of vertical images. Hence, the quantitative image stage in which intersection densities have to be determined in orthogonal directions should not be executed with high grid density. So, the simple job can be best accomplished manually on analogue images. Alternatively, these orthogonal measurements when obtained on digitized images - in which the direction of digitization is adjusted to prevailing crack direction - can equally be used for unbiased estimation of damage characteristics, as demonstrated herein.

6 Conclusions

Spatial damage structures can be analyzed in practice by quantitative image analysis based on a sweeping test line system. For the practical cases of prevailing compressive or tensile loadings, (a set of) *vertical* sections will do, restricting dramatically efforts required for preparation of samples and image analysis. Otherwise random sampling would be required, with dramatic economic consequences. Alternatively, it is proposed by Ringot and Bascoul [2001] degenerating the basic stereological relationship that is also used in this paper ($S_V = 2\overline{P}_L = (4/\pi)L_A$) into $S_V = L_A$. This is an illogical and inaccurate manipulation and demonstrated herein to be unnecessary when the S/S-concept is accepted as a much better approximation of the actual situation.

The choice to automate the quantitative image analysis operation is a risky one, because characteristic measures for the damage structure, like total crack length (or specific crack surface area) and degree and direction of prevailing crack orientation will be seriously biased [Bisschop 2002].

The quantitative image analysis operation can be restricted to only vertical section images, when, instead, the S/S-concept of a partially linear or partially planar dispersion of surfaces in space is adopted (for situations where compressive and tensile stresses

dominate, respectively). Moreover, the direction of (four-connexity) digitization of the vertical images has to be adjusted (approximately) to the prevailing crack orientation direction, so that the measurements can be restricted to two orthogonal intersection counting operations of grid lines and cracks.

These observations are unbiased when use is made of analogue or digitized images, so that unbiased estimates of total crack length in 2D or specific crack surface area in 3D can be obtained.

Crack orientation distribution *measurements* on digitized images will always be biased to an unknown degree unless methods compensating for digitalized pixel direction, such as the S/S-concept for a partially oriented crack structure, are taken into account.

The economy of the four-stage sampling scheme, aiming to link crack measurements to the behavior of the engineering concrete structure under load, favors limitation of the number of observations in the last stage, the quantitative image analysis operation. Hence, the simple counting operation of limited extent can be manually executed as well.

Literature

Ammouche, A., Breysse, D., Hornain, H., Didry, O. and Marchand, J. (2000). A new image analysis technique for the quantitative assessment of microcracks in cement-based materials. *Cem. Concr. Res.* 30(1): 25-35.

Bentz, D.P., Garboczi, E.J. and Stutzman, P.E., Computer modeling of the Interfacial transition zone in concrete, *Interfaces in Cementitious Composites,* E&FN Spon, London, 107-116, 1993.

Bisschop, J., *Drying shrinkage microcracking in cement-based materials*. Ph.D. thesis, Delft University of Technology, the Netherlands, 2002.

Carcassès, M., Ollivier, J.P. and Ringot, E. (1989). Analysis of microcracking in concrete. *Acta Stereol*. 8(2): 307-312.

Carpinteri, A. and Puzzi, S. (2009). The fractal-statistical approach to the size-scale effects on material strength and toughness. *Prob. Engr. Mech.* 24(1): 75-83.

Chaix, J.M. and Grillon, F. (1996). On the rose of direction measurements on the discrete grid of an automatic image analyzer. *J. Microsc.* 184: 208-213.

Chen, H., Stroeven, P., Ye, G., Stroeven, M. (2006). Influence of boundary conditions on pore percolation in model cement paste. *Key Engr. Mat.* 303: 486-492.

Darwin, D., Abou-Zeid, M.N. and Ketcham, K.W. (1995). Automated crack identification for cement paste. *Cem. Concr. Res.* 25: 606-616.

Fu, G. and Dekelbab, W. (2003). 3-D random packing of polydisperse particles and concrete aggregate grading. *Powd. Techn.* 133(1-3): 147-155

Grutzeck, M.W., Shi, D., Liu, G. and Kwan, S. (1993). Computer simulation of interfacial packing in concrete. *J. Mat. Sci.* 28(3) 444-450.

Gundersen, H.G. and Osterby, R. (1981). Optimizing sampling efficiency of stereological studies in biology, or: "Do more less well". *J. Microsc.* 121: 65-73.

He, H. (2010). *Computational modelling of partical packing in concrete*. Ph.D. thesis, Delft University of technology

Howard C.V. and Reed M.G. *Unbiased Stereology:Three-dimensional Measurement in Microscopy,* BIOS Scientific Publishers, 2005.

Maletti, G.M. and Wulfsohn, D. (2006). Evaluation of variance models for fractionator sampling of trees. *J. Microsc.* 222: 228-241.

Nemati, K.M. (1994). *Generation and interaction of compressive stress-induced microcracks in concrete*. Ph.D. thesis, University of California, USA.

Nemati, K.M. and Stroeven, P. (2000). Stereological analysis of micro-mechanical behaviour of concrete. *Mat. Struct.* 34: 486-494.

Reinhardt, H.W., Stroeven, P., den Uijl, J.A., Kooistra, T.R. and Vrencken, J.H.A.M. (1978). Einfluss von Schwingbreite, Belastungshöhe und Frequenz auf die Schwingfestigkeit von Beton bei niedrigen Bruchlastwechselzahlen. *Betonw. & Fertigteil-Techn.* 44: 498-503.

Ringot, E. (1988). Automatic quantification of microcracks network by stereological method of total projections in mortars and concrete. *Cem. Concr. Res.* 18: 35-43.

Ringot, E. and Bascoul, A. (2001). About the analysis of microcracking in concrete. *Cem. Concr. Comp.* 23(2/3): 261-266.

Saouma, V.E., Barton, C.C. and Gamaleldin, N.A. (1990). Fractal characterization of fracture surfaces in concrete. *Engr. Fract. Mech.* 35: 47-53.

Stroeven, P. (1973). *Some aspects of the micromechanics of concrete.* Ph.D. thesis, Delft University of Technology

Stroeven P. (1979). Geometric probability approach to the examination of microcracking in plain concrete. *J. Mater. Sci.* 14: 1141-1151.

Stroeven, P. (1982). Structural modelling of plain and fibre reinforced concrete. *J. Comp.* 13: 129-139.

Stroeven, P. (1990). Some observations on microcracking in concrete subjected to various loading regimes. *Engr. Fract. Mech.* 35(4/5): 775-782.

Stroeven, P. (2009). Methodology of damage assessment in concrete. Scope and restrictions. *Proceedings International Conference on Fracture* (12th ICF), Ottawa, (available on CD).

Stroeven, P., Guo, Z. (2006). Modern routes to explore concrete's complex pore space. *Im. Anal. Stereol.* 25(2): 75-85.

Stroeven, P. Hu, J. (2007). Gradient structures in cementitious materials. *Cem. Concr. Comp.* 29: 313-323.

Stroeven, P., Stroeven, A.P., and Dalhuisen, D.H. (2001). Image Analysis of "natural" concrete samples by automated and manual procedures. *Cem. Concr. Comp.* 23: 227-236.

Stroeven, A.P., Stroeven, P., van der Meer, J.J.M. (2005). Microfabric analysis by manual and automated stereological approaches: a methodological approach to Antarctic tillite. *Sediment.* 52: 219-233.

Stroeven, P., Hu, J., Stroeven, M. (2009). On the usefulness of discrete element computer modelling of particle packing for materials characterization in concrete technology. *Comp. Concr.* 6(2): 133-153.

Stang, H., Mobasher, B. and Shah, S.P. (1990). Quantitative damage characterization in polypropylene fibre reinforced concrete. *Cem. Concr. Res*. 20: 540-558.

Underwood, E.E. *Quantitative Stereology,* Addison-Wesley, Reading, MA, 1970.

Wang, Y. and Diamond, S. (2001). A fractal study of the fracture surfaces of cement pastes and mortars using a stereoscopic SEM method. *Cem. Concr. Res.* 31: 1385-1392.

Wulfsohn, D., Maletti, G.M. and Toldam Andersen, T.B. (2004). Unbiased estimator for the total number of flowers on a tree. *Acta Hort.* 707: 245–252.